Journal of Non-Crystalline Solids 594 (2022) 121803

Contents lists available at ScienceDirect

Journal of Non-Crystalline Solids

journal homepage: www.elsevier.com/locate/jnoncrysol

Energy-band-structure calculation by below-band-gap spectrophotometry in thin layers of non-crystalline semiconductors: A case study of unhydrogenated *a*-Si

M. Ballester [a], A.P. Márquez [b], C. García-Vázquez [b], J.M. Díaz [b], E. Blanco [c], D. Minkov [d], S.M. Fernández-Ruano [e], F. Willomitzer [f], O. Cossairt [a,f], E. Márquez [c,*]

[a] Department of Computer Science, Northwestern University, USA
[b] Departamento de Matemáticas, Universidad de Cádiz, Spain
[c] Departamento de Física de la Materia Condensada, Universidad de Cádiz, Spain
[d] College of Energy and Electronics, Technical University of Sofia, Bulgaria
[e] Photovoltaic Solar Energy Unit, Energy Department, CIEMAT, Spain
[f] Department of Electrical and Computer Engineering, Northwestern University, USA

ARTICLE INFO

Keywords:
Amorphous semiconductors
Optical properties
Thin-film characterization
Wemple–DiDomenico model
Effective-medium theories

ABSTRACT

We have in depth analyzed the refractive-index behavior and optical absorption of below-band-gap light, in order to calculate the basic parameters of the energy-band structure of thin layers of non-crystalline semiconductors. By carrying out a semi-empirical determination of the influence of the finite (non-zero) width of the valence and conduction electronic bands, we find the dependence of the index of refraction upon the photon energy, $n(E)$, which goes just one order beyond the Wemple–DiDomenico two-level single-oscillator expression, and we simultaneously obtain the spectral dependence of the absorption coefficient, $\alpha(E)$. By model fitting the measured normal-incidence transmittance spectrum, we demonstrate that with a highly-sensitive double-beam spectrophotometer, it can be accurately determined the energy distance, $E_{M,Sol}$, between the corresponding 'centers of mass' of the bonding and anti-bonding electronic bands, and also a reasonable estimate of the so-called *effective* width, Δ_{eff}, of both valence and conduction bands. We have used this devised optical approach with a series of uniform and non-uniform thin layers of unhydrogenated fully *a*-Si, grown by RF-magnetron-sputtering deposition, onto room-temperature transparent glass substrates. The advantages of our novel approach are mainly due to the additional attention paid to the roles of the weak-absorption Urbach tail and the thickness non-uniformity of the studied *a*-Si films. We have also used a universal normal-incidence transmission expression reported by the authors in an earlier paper, which can be applied even to strongly-wedge-shaped semiconductor layers. Together with the use of the improved Solomon formula for the normal optical dispersion of the refractive index, the complete approach with all its elements constitutes the main novelty of the present paper, in comparison with other existing works.

1. Introduction

Ultraviolet–visible–near-infrared (UV–Vis–NIR) spectrophotometry, at normal incidence, is frequently employed for accurately determining both the optical and the structural properties and also the morphology of uniform and non-uniform thin layers of amorphous semiconductors [1–7]. Concretely speaking, by the use of the optical transmittance spectrum only, measured with a highly-sensitive, double-beam ratio-recording spectrophotometer, we can determine the geometrical parameters, average film thickness, $\bar{d}$, and film thickness variation, Δd, the optical constants, refractive index and extinction coefficient, n and k, respectively, and the Tauc optical gap, E_{opt}, of a non-crystalline semiconducting layer under study. The value of this last particular optical parameter, E_{opt}, is found after the calculation of the optical-absorption coefficient, $\alpha(\lambda)$, as a function of the corresponding free-space wavelength, λ.

For the specific case of an average layer thickness larger than the incoming-photon wavelength, the experimentally-measured transmittance spectrum exhibits a characteristic oscillatory behavior, and from the respective maxima and minima of this Fabry–Perot (FP) interference fringes, a precise and accurate spectral dependence (or optical dispersion) $n(\lambda)$ or $n(E)$, can be determined ($E = \hbar\omega$ is the

* Corresponding author.
E-mail address: emilio.marquez@uca.es (E. Márquez).

https://doi.org/10.1016/j.jnoncrysol.2022.121803
Received 19 April 2022; Received in revised form 1 July 2022; Accepted 6 July 2022
Available online 21 July 2022

incident-photon energy) [1–7]. On the other hand, in previous works reported by Solomon et al. [8–10], very interestingly, the dispersion of the index of refraction was utilized in order to obtain the so-called 'average gap', E_M, an optical quantity associated with the energy-band structure of the amorphous-semiconductor material. Particularly, this entirely empirical quantity has been demonstrated to be a measure of the energy difference between of the 'centers of mass' of the valence and conduction energy bands, accompanied by the necessary weighting factors, of the non-crystalline semiconductor. Furthermore, going one significant step further, its corresponding bandwidth was also reasonably estimated from the normal dispersion of the index of refraction. Hence, with straightforward normal-incidence transmission measurements, it can be found highly valuable information about the energy-band structure of the non-crystalline solid.

In this paper, by the in-depth study of the photon energy dependence of the refractive index, $n(E)$, we have been able to calculate not only the energy distance E_M between the centers of the bonding and anti-bonding electronic bands but also the corresponding *effective* width, Δ_{eff}, of these two energy bands of the semiconductor. The present approach, mainly based upon the Solomon optical-dispersion model, can be applied in principle to any uniform and non-uniform film of an amorphous semiconductor, and the experimental results obtained and discussed in detail in this work belong to both uniform and non-uniform layers of the prototypical hydrogen-free amorphous silicon (*a*-Si), grown in this investigation by the radio-frequency magnetron-sputtering deposition technique (RFMS), onto transparent glass substrates, at room temperature.

In the last few decades, *a*-Si has been gaining more relevance, generally speaking, in the field of solar cells [11–16]. The hydrogenless *a*-Si is proposed to the precursor material in order to prepare recrystallized silicon (using to that end a laser source), that can substitute the *c*-Si as a solar absorber. During the crystallization process it is found a polycrystalline material which is made up of crystalline grains whose sizes are of the order of microns, ant they can be visualized with the naked eyes. It is a novelty the fabrication of the *a*-Si precursor material by radio-frequency magnetron sputtering, and also at relatively low temperature, smaller than around 300 °Celsius. An additional advantage of the sputtering deposition method is that such a technique avoids the use of toxic gases during the growth process, which makes it certainly more friendly to the environment. And last but not least, it has to be stressed that on this way very small thickness of only around 10 μm are needed. It favorably compares with the silicon wafers whose thickness ranges between 100 and 180 μm. That is to say, there is a remarkable reduction of the solar absorber thickness, and it obviously means an important reduction of cost.

In addition, multi-layered H-free *a*-Si thin films have become in the last decade a certainly promising candidate for Li-ion battery anodes, for it was found to be a reversible host material for Li intercalation, and it possesses a theoretical specific capacity of approximately 4200 mA h/g, the highest known value among all the existing material in nature [17]. Moreover, it was reported by Karabacak and Demirkan [18] a low-cost and scalable procedure of producing hydrogen-less *a*-Si-thin-layer anodes, with large specific-capacity values and large numbers of charging/discharging cycles. Unhydrogenated *a*-Si thin layers were grown for such a goal, with a mass–density-modulated multilayer structure, and these *a*-Si films were prepared by a high/low working-pressure RF magnetron sputtering deposition method.

To end this introduction, it is worthy to underline that, to the best of the authors' knowledge, this is the first time that our adopted approach, formed by the particular combination of both the Solomon dispersion model [10] and the consideration of the non-negligible absorption associated to the Urbach tail [19,20], along with the use of both the inverse-synthesis method [21,22] and a novel universal formula for the normal-incidence transmission [5], has all been applied to films of amorphous semiconductors in order to determine their *energy-band structure*. This presented original combination of the Solomon formula and the Urbach rule will be designated from now on, the 'Solomon–Urbach model'.

2. Experimental procedure: Preliminary surface, structural and optical characterizations of *a*-Si layers

First of all, it must be noted that the preparation of the *a*-Si thin-film specimens under study by room-temperature, radio-frequency magnetron sputtering deposition technique, has been extensively reported by us elsewhere [23–25], and there is no need to be repeated here.

The quality of the surface morphology, quantified by the root-mean-square value of the surface roughness, R_q, of the studied *a*-Si films, was measured by atomic force microscopy (AFM microscopes Bruker Nanoscope IIIA). The representative AFM micrograph in Fig. 1 proves that our *a*-Si specimens do have a flat, shiny, and smooth surface. The AFM measurements show that the value of the surface-roughness parameter, R_q, is about 1.50 nm. On the other hand, the value of this parameter R_q for the 1-mm-thick glass substrate was found to be around 0.60 nm.

It must also be noted the characteristic surface effect, usually called 'broccoli', 'orange peel', or 'dry mud' cracks [26], seen in the top-view SEM image (SEM: FEI Nova NanoSEM 450), belonging to a representative *a*-Si specimen, and displayed in Fig. 1. To date there is no clear explanation, whatsoever, of the possible underlying mechanisms that could give a concluding explanation of the formation of this very peculiar surface effect. However, it might be reasonably proposed that it could be correlated to the expected tendency of shrinkage of any thin coating film, in order to reduce its associated surface energy, and so, would be caused by the existing tensile internal stresses within the thin layer, occurring during the RFMS coating process.

In addition, the optical constants, refractive index, n, and extinction coefficient, k, were accurately calculated from room-temperature measurements of the normal-incidence transmission spectrum of each *a*-Si specimen to be studied. Those optical spectra were measured by a Perkin-Elmer 1050 and/or a Cary 5000 UV/Vis/NIR, double-beam ratio-recording spectrophotometer, both state-of-art instruments. The specific irradiated area of the *a*-Si specimen was 1 cm × 1 mm, and the adopted spectral width was 2 nm. The transmission data, on the other hand, were collected with a data interval of 4 nm. All the normal-incidence transmittance spectra were measured from 300 to 2500 nm. It has to be noted that various spots on each *a*-Si specimen investigated have been illuminated, and we have indeed found excellent consistency between the results from the various spot-to-spot transmission measurements. Moreover, the value of optically-calculated average layer thickness was routinely confirmed by the respective cross-sectional SEM micrographs and also cross-checked for a few chosen *a*-Si specimens by a Veeco Dektak 150 mechanical profilometer. It should be stressed that the difference found with the value of the average layer thickness exclusively determined from the transmission measurements only was, for the particular specimens selected, lower than around 3 %.

In order to study the non-crystalline atomic structure of the investigated sputtered *a*-Si specimens, the first-order Raman spectra, measured at room temperature, of the present *a*-Si thin layers, were excited with a 633-nm laser of 20-nW nominal power by employing a Horiba LabRAM HR Raman spectrometer. In Fig. 1, it is shown three typical Raman spectra for the representative *a*-Si samples, respectively.

Let us commence now with the detailed analysis of those as-measured first-order Raman spectra. It is interesting to recall that in a material, a small part of the incident photon energy can be employed in order to produce a lattice vibration (that is to say, a phonon quasiparticle). The rest of the energy escapes as a photon, with slightly lower energy in comparison with that of the incoming photon, and this particular energy shift is the so-called Raman shift. In the specific case of the *a*-Si material, the momentum selection rules is considered to be relaxed, as compared to that of the single-crystalline Si, and thus various phonon modes, and their respective energies, are now allowed. Generally speaking, a broad peak centered at about 480 cm^{-1}, almost dominates the complete first-order Raman spectrum. It is noticed that the three typical Raman spectra for three representative

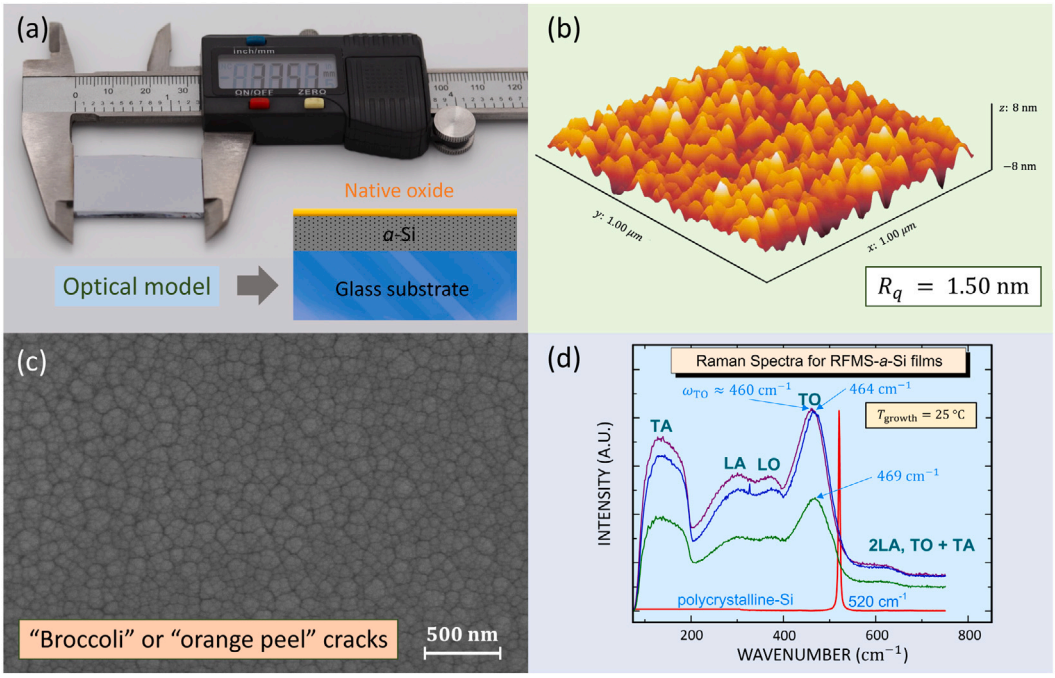

Fig. 1. (a) The ordinary visual appearance (unaided eye) of the surface of a representative *a*-Si specimen (see also the displayed three-layer optical model for our studied samples). (b) AFM and (c) top-view SEM images of the specimen #3. The displayed top-view SEM image clearly illustrates the 'broccoli', 'orange peal', or 'dry mud' cracks, characteristic of the *a*-Si thin layers under investigation. (d) Three typical Raman spectra corresponding to three *a*-Si thin-film samples, respectively, all them sputtered onto room-temperature glass substrates, are shown. (Adapted from [25] by E. Marquez et al.).

specimens depicted in Fig. 1, exhibits the main peak at a particular average value of $\omega_{TO} = 464\,cm^{-1}$, associated with the transverse-optic (TO) phonon band, and another main peak at a particular value of the wavenumber of around $140\,cm^{-1}$, corresponding in this other case to the transverse-acoustic (TA) phonon-band [27–29]. Along with these two dominant Raman peaks, two more Raman peaks belonging, firstly, to the longitudinal-optic (LO) phonon band, and positioned at around $372\,cm^{-1}$, and, secondly, to the longitudinal-acoustic (LA) phonon band, positioned in this other case at a smaller value of about $300\,cm^{-1}$, are also observed. Furthermore, it has to be mentioned that the broad but small characteristic feature seen at the high-energy side, in those representative *a*-Si first-order Raman spectra shown in Fig. 1, at a particular value of the wavenumber of nearly $620\,cm^{-1}$, can be associated to two plausible *two-phonon* excitations, such as TO+TA and 2LA, respectively [27–29].

The TA-peak intensity, I_{TA}, considered in relation to the TO-peak intensity, I_{TO}, on the other hand, is well accepted to quantify the degree of the extent of the medium-range order existing in the atomic structure of a disordered solid. Thereby, the higher the intensity ratio, γ_{Raman} ($= I_{TA}/I_{TO}$), the lower the amount of medium-range order occurring in such a solid. For the *a*-Si specimen #1, γ_{Raman} was found to be as large as 0.89, whereas the value of the parameter γ_{Raman} for a sputtered *a*-Si (but in this case grown without the RF magnetron enhancement existing during the deposition of our samples) was reported to be a slightly lower value of 0.80. Additionally, Orapunt et al. [30–32], fabricated a novel form of *a*-Si by the deposition technique of ultra-high-vacuum evaporation of Si atoms, onto a room-temperature quartz substrate, whose corresponding thin-layer mass density resulted to be surprisingly just only 2 % smaller than that of *c*-Si, and possessing a lower value of the structural parameter γ_{Raman} of 0.70. Hence, from the standpoint of their non-crystalline atomic structure, it is then reasonable to think that our RFMS *a*-Si specimens are, indeed, the most disordered of all the above-mentioned and differently-deposited *a*-Si thin-films materials.

Grazing-incidence X-ray diffraction (GIXRD) measurements made previously on the RFMS-*a*-Si specimens have undoubtedly corroborated their non-crystalline nature, with none of the characteristic sharp X-ray diffraction peaks of its *c*-Si counterpart being present, at all, in the bulk of the thin-film sample [25]. The GIXRD and EDX measurements also demonstrated the total absence of any kind of impurities in the investigated *a*-Si layers. Moreover, micro X-ray diffraction (μXRD) measurements were carried out, in order to get an even much deeper insight into the atomic structure and morphology of sputtered *a*-Si layers. This particular experimental technique permits the detection of very minor changes that are not possible to be observed with other experimental configurations. Three crystalline peaks were noticed in the μXRD pattern, which were attributed to an SiO_2 native oxide overlayer, very likely to be a priori expected in the RFMS-*a*-Si films [16]. Three possible candidate crystalline structures were those of the quartz, tridymite, and cristobalite, respectively. It should be mentioned that Morita et al. [33] reported the appearance of crystalline SiO_2, up to 2 nm thick, also detected by XRD measurements, at the interfaces, and formed by thermal oxidation.

3. The single-effective-oscillator model

Even though the refractive-index dispersion of amorphous semiconductors can be accurately described in the sub-band-gap region by the two- or three-term Cauchy equations, it is difficult to assign a physical interpretation to these simple expressions. Hence, we take into consideration another expression, which can be correlated to physical parameters, in a much more straightforward fashion. So, the real part of the electronic dielectric function in most covalent and ionic, both ordered and disordered solids can be written as follows,

$$\varepsilon_1(\omega) = 1 + \frac{e^2}{\pi^2 m} \sum_{i,j}{}' \int_{BZ} d^3k \frac{f_{ij}^{\alpha}(\mathbf{k})}{\omega_{ij}^2(\mathbf{k}) - \omega^2}, \tag{1}$$

where e and m are the electron charge and mass, respectively. On the other hand, the sum extends over all the energy bands i and j, such that it is verified that $i \neq j$, and extends over the whole volume of the (first) Brillouin zone (BZ, a unit cell of the reciprocal or **k**-space). For each electronic transition between two energy bands i and j, respectively, the corresponding oscillator strength for a specific polarization of the electric field of light of a particular direction α is expressed by $f_{ij}^{\alpha}(\mathbf{k})$. In

order to simplify Eq. (1) to convenient macroscopic optical parameters that can be instead experimentally measured, it should be stressed that isotropic two-band models, despite their great simplicity, have been found to be an excellent approximation, in many cases [8,34,35]. Thus, the isotropic models must be particularly suitable for non-crystalline materials as a result of their lack of long-range structural order. By using the Wemple–DiDomenico's highly-simplified dispersion model, which reduces the complex valence- and conduction-band system of a real semiconductor to just a two-energy-level system, it can be demonstrated that the previous expression of $\varepsilon_1(E)$, Eq. (1), can be finally reduced to an approximate, single-effective-oscillator formula, accounting for the dielectric response for the sub-band-gap electronic transitions:

$$\varepsilon_1(E) = n^2(E) = 1 + (n^2(0) - 1)\frac{E_{\mathrm{M,WD}}^2}{E_{\mathrm{M,WD}}^2 - E^2}. \tag{2}$$

Here $n(E)$ is the expression of the refractive index as a function of the photon energy, and $n(0)$ is the value of the refractive index extrapolated to zero energy (infinite wavelength), i.e., the static refractive index. The physical quantity $E_{\mathrm{M,WD}}$ is the average energy-gap parameter, which corresponds in this particular optical-dispersion model to the energy difference between the assumed two energy levels of the single-oscillator system (Fig. 3(a)). In fact, it has to be added that it is physically clear that the parameter $E_{\mathrm{M,WD}}$ does not correspond to an actual energy-band gap, being instead similar to the energy parameter (the so-called 'Penn gap'), used by Penn [36] for the determination of the static refractive index, $n(0)$, in semiconductors. It is clear that this parameter $E_{\mathrm{M,WD}}$ is a kind of measure of the energy difference between the 'centers of mass' of the valence (bonding) and conduction (anti-bonding) bands. The derivation of the two optical parameters $n(0)$ and $E_{\mathrm{M,WD}}$ from first principles, by using Eq. (1), is most certainly excessively ambitious in the case of a disordered solid, where little is known on the transition probabilities of both localized as well as extended energy-band states. It must also be pointed out that the experimental spectral dependence of the refractive index, $n(E)$, can deviate from that expressed by Eq. (2), when the photon energy gets close to the value of the actual optical gap, E_{opt}. The single-oscillator model then is not obeyed, and the existence of a non-zero bandwidth gives place to significant discrepancies, as a result of the denominator term in Eq. (2); it can be anticipated a change in the spectral dependence $n(E)$ quicker than that exhibited by Eq. (2), which is certainly what has often been experimentally measured [34]. However, this experimental spectral dependence $n(E)$ has been found to be more gradual and smooth in the case of the hydrogenless *a*-Si material under study. In spite of that, we will be able to present below valuable information on the real width of the valence and conduction energy bands of this unhydrogenated *a*-Si.

For values of the photon energy, much smaller than the value of the optical gap, E_{opt}, Eq. (2) gave rise to an excellent experimental fit to previously-determined values of the refractive index, by the authors of this paper, of hydrogen-free *a*-Si [23], by using a direct dispersion-model-free approach. On the other hand, the average gap, $E_{\mathrm{M,WD}}$, offers relevant quantitative information on the overall electronic-band structure of the amorphous material, certainly quite different from that by the optical gap, E_{opt}, which only probes the optical properties in the proximity of the energy-band edges of the semiconductor. Particularly, the localized electron states near the valence and conduction energy bands (the so-called 'tail electronic states'), can have a notable influence on the optical absorption of the material, and therefore remarkably decrease the value of E_{opt}, while, on the contrary, they can influence the normal dispersion of the refractive index of the sub-band-gap light, in a small fashion. Thus, they could enlarge the so-called 'Urbach–Martienssen's tails', or more simply, 'Urbach tail' [19,20], but would not significantly modify the value of the average energy gap, $E_{\mathrm{M,WD}}$.

It has to be indicated that in our method of analysis, contrariously to what is done by Solomon [10], we shall also interpret, in terms of the porosity, the calculated value of the static refractive index, $n(0)$, which has been determined, as said before, by employing our relatively simple semi-empirical arguments. This optical parameter $n(0)$ had been considered, in this context, only an experimentally-determined free parameter that will be found by computationally fitting the as-measured normal-incidence transmission spectrum of the specimen by using to that end the Nelder–Mead numerical method (also called the downhill simplex method). The computed value of $n(0)$ was also experimentally cross-checked by making use of a far-infrared spectrometer.

4. Determination of optical properties of amorphous semiconductor films

4.1. Calculations of $\bar{d}$, Δd, $n(0)$, $E_{\mathrm{M,WD}}$, α_0, and E_{U} by fitting of the universal transmission formula to the as-measured spectrum

The optical transmission expression, $T_{\Delta d}(\lambda)$, used in this work, is a new equation, which has been recently reported by the authors of the present paper [5,25]. These universal formulae of the normal-incidence transmittance for a real, highly-non-uniform (strongly-wedge-shaped) thin weakly-absorbing film, onto a thick transparent substrate, is as follows:

$$T_{\Delta d}(\lambda; n(\lambda), k(\lambda), s(\lambda), \bar{d}, \Delta d) = \frac{A\left[\left(\arctan\left(\frac{C}{D}\right) + N_{\mathrm{c},2}\pi\right) - \left(\arctan\left(\frac{B}{D}\right) + N_{\mathrm{c},1}\pi\right)\right]}{D(\varphi_2 - \varphi_1)} x_{\mathrm{average}}, \tag{3}$$

where

$$\begin{aligned}
A &= 32(n^2 + k^2)s,\\
B &= x_{\mathrm{average}}(F + E(G + Hx_{\mathrm{average}}))\tan(\varphi_1/2),\\
C &= x_{\mathrm{average}}(F + E(G + Hx_{\mathrm{average}}))\tan(\varphi_2/2),\\
D &= \sqrt{E^2 - x_{\mathrm{average}}^2(F^2 + G^2 - 2EH - H^2x_{\mathrm{average}}^2)},\\
E &= \left((n+1)^2 + k^2\right)\left((n+1)(n+s^2) + k^2\right),\\
F &= 2k\left(2(n^2 + k^2 - s^2) + (n^2 + k^2 - 1)(s^2 + 1)\right),\\
G &= 2\left((n^2 + k^2 - 1)(n^2 + k^2 - s^2) - 2k^2(s^2 + 1)\right)\times\\
&\quad \left((n-1)(n - s^2) + k^2\right),\\
H &= (n-1)^2 + k^2,\\
\varphi_1 &= 4\pi n(\bar{d} - \Delta d)/\lambda,\\
\varphi_2 &= 4\pi n(\bar{d} + \Delta d)/\lambda,\\
\alpha &= 4\pi k/\lambda,\\
x_{\mathrm{average}} &= \exp(-\alpha\bar{d}),
\end{aligned}$$

and where lastly the two introduced correcting integers, $N_{\mathrm{c},1}$ and $N_{\mathrm{c},2}$, respectively, are given by the respective two expressions:

$$N_{\mathrm{c},1} = \mathrm{round}(\varphi_1/2\pi),$$

and

$$N_{\mathrm{c},2} = \mathrm{round}(\varphi_2/2\pi).$$

The newly-defined function, 'round', does round off its corresponding arguments to its closest integer values. The novel general expression of the transmission, Eq. (3), is, importantly, a *continuous* function that can be used in order to perform the complete optical characterization of a wide variety of thin-film non-crystalline semiconductors, with high accuracy. Furthermore, the so-far existing limiting maximum value of the non-uniformity parameter, $\Delta d_{\mathrm{max}} = \lambda/4n$ [5], when rigorously trying to determine the optical constants of strongly-wedge-shaped films, has been now successfully suppressed, with the introduction of the previous two angle parameters, $N_{\mathrm{c},1}$ and $N_{\mathrm{c},2}$, respectively, in the universal formulae for the normal-incidence transmittance, Eq. (3).

In our analysis of the experimental transmission spectrum, we do take into consideration the existence of the exponential Urbach spectral

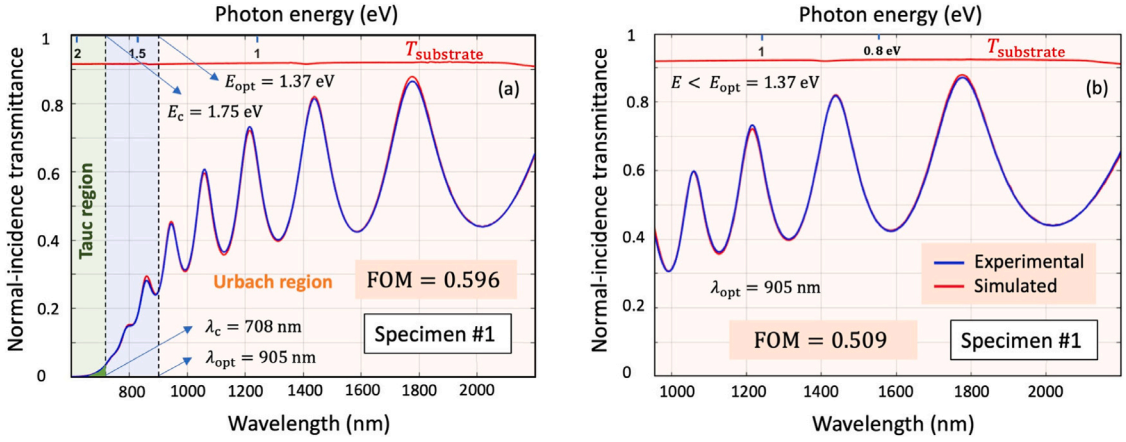

Fig. 2. (a) Experimental (red line) and best-WD-model-fit (blue line) normal-incidence transmission spectra of the *a*-Si specimen #1. Measured (red line) transmission spectrum of the glass substrate alone is compared with the two former spectra. Very importantly, the value of the so-called connection energy, E_c of 1.75 eV, which defines the transition from Urbach to Tauc-Lorentz functionalities [25] is indicated (the very small green area represents the Tauc region). (b) The excellent comparison between the simulated and measured transmission spectra in only the sub-band-gap region is clearly illustrated in this figure. (For interpretation of the references to color in this figure legend, the reader is referred to the web version of this article.)

region, where the absorption is *not* negligible, on the contrary, to what was assumed in Ref. [10]. The transmittance is as aforementioned a function of $\bar{d}$, Δd, $n(\lambda)$ and $\alpha(\lambda)$ (we have initially determined the corresponding values of the refractive index of the transparent glass substrate, $s(\lambda)$, onto which the sputtered *a*-Si film was grown, from previous transmission measurements of such a bare substrate). If the expression of the normal dispersion of the refractive index given by Eq. (2) is adopted, then the theoretical transmission equation employed will finally depend upon six free parameters: $\bar{d}$, Δd, $n(0)$, $E_{M,WD}$, α_0 and E_U. We will next determine those six free parameters by direct computer fitting of the previous expression for $T_{\Delta d}(\lambda)$ to the as-measured transmittance spectrum by using the devised computer program 'AdjusTransIS toolbox', based on the Matlab (R2022a) software package.

This procedure, named inverse synthesis, an alternative to the use of the FP interference fringes, following the Swanepoel envelope method, has the important advantage of being able to be applied to very thin layers, with their corresponding average thicknesses lower than around 100 nm. In these circumstances, the number of oscillations is unfortunately quite small or nonexistent. Moreover, special care has to be taken when employing this reverse-engineering approach, considering that this method is based upon the magnitude of the transmission, $T_{\Delta d}(\lambda)$, instead of the wavelength positions, λ_{tan}'s, of the corresponding extrema of the FP interference pattern, and it is therefore relevant that the transmittance measurement is both precise and accurate. With a standardized state-of-art double-beam spectrophotometer, and after the necessary thermal stabilization period, the overall transmission measurement error is diminished down to a value of less than approximately 1×10^{-4}.

In order to illustrate the application of this model-fitting procedure, it has been in depth analyzed a layer of non-hydrogenated *a*-Si, in this case with many FP oscillations in the whole spectral range, with $\lambda \gtrsim 700$ nm (Fig. 2(a)). It must be emphasized that there is practically *non-negligible* weak absorption in the complete wavelength range shown in Fig. 2. This existing absorption is the universal observed characteristic feature of the optical-absorption spectra close to the band edges observed in both crystalline and amorphous semiconductors, and as already mentioned, is the Urbach–Martienssen exponential absorption edge. The absorption coefficient, α, for optically-induced electronic transitions from the valence- up to the conduction-band tails, obeys the well-known rule: $\alpha(E) = \alpha_0 \exp(E/E_U)$, where α_0 is a constant and E_U is the Urbach energy. The introduction of this Urbach relationship in the dispersion-model fit is a novelty of our approach, as compared with some others reported works. The values of $n(0)$, $E_{M,WD}$, and E_U, computed from our model fit, and all of them listed in Table 1, are in excellent agreement with those calculated from only extrema of the interference pattern by using the Swanepoel model-free graphical method [2]. Very interestingly, the value of energy parameter, the so-called connection energy, E_c, of 1.75 eV (λ_c = 708 nm), in the case of specimen #1, which marks the transition from the Urbach tail to the Tauc-Lorentz functionalities [25], is shown in Fig. 2(a). The introduced small green area corresponds to exclusively the Tauc spectral region, while the light blue one refers to those values of the photon energy within the specific range, $E_{opt} < E < E_c$. This very fact explains the a priori rather unexpected success of the proposed combination of the sub-band-gap Wemple–DiDomenico model, plus the Urbach rule, for taking into account the non-negligible absorption in the sputtered a-Si material. This is certainly true when calculating the optical properties of the present unhydrogenated a-Si, in the whole measurement spectral range from a vacuum wavelength of around 700 nm, in the particular case of specimen #1 displayed in Fig. 2(a).

4.2. AdjusTransIS Toolbox: Matlab-coded program for the optical characterization of non-crystalline semiconductor layers

The Matlab computer program called 'AdjustTransIS Toolbox', developed in order to carry out the accurate optical characterization of both parallel-faced and wedge-shaped amorphous semiconductor thin films, falls, as above-mentioned, into the category of reverse or inverse-synthesis approach. The simplified flowchart of its algorithm was already reported in [5], and it has to be also indicated that the AdjusTransIS toolbox is fully configurable by employing MS-Excel files. This toolbox allows fast fitting a model-generated transmission spectrum to the experimental data corresponding to a semiconducting film, by adjusting to that end up to a maximum possible number of *nine* free parameters. Up to *seven* of them belong to the adopted dispersion mode, plus *two* geometrical parameters, namely, the average layer thickness and, very significantly, the homogeneity parameter, $\bar{d}$ and Δd, respectively.

The main idea behind 'AdjustTransIS Toolbox', in order to be able to compute all the model parameters, is to find the whole set of values minimizing the following figure-of-merit (FoM) function:

$$\mathrm{FoM}(T) = 100 \times \mathrm{RMSE} = 100 \sqrt{\frac{\sum_{i=1}^{N} \left(T_{i,\mathrm{meas}} - T_{i,\mathrm{simu}}\right)^2}{N_{\mathrm{exp}}}}, \tag{4}$$

where N_{exp} denotes the total number of experimentally-measured data points, $T_{i,meas}$, stands for each as-measured transmission value, and,

Table 1
Values of the WD single-effective-oscillator model parameters, $n(0)$ and $E_{M,WD}$, respectively, for three *a*-Si thin films, sputtered with increased Ar-gas pressure (p_{Ar}) . The geometrical parameters $\bar{d}$ and Δd are the average layer thickness and the wedging parameter, respectively. E_U is the Urbach energy, and FoM is the obtained value of the figure of merit corresponding to each *a*-Si specimen.

a-Si specimen ID	p_{Ar} (Pa)	$n(0)$	$E_{M,WD}$ (eV)	E_U (meV)	$\bar{d}$ (or d) (nm)	Δd (nm)	$\bar{d}_{SEM}$ (nm)	FoM
#1	4.4	**3.10**	**3.28**	**241**	1121	0	1130	0.599
#2	3.2	**3.15**	**3.26**	**249**	769	25	777	0.447
#3	2.4	**3.33**	**3.17**	**221**	1175	0	1167	0.658
device-grade *a*-Si:H [10]	N.A.	**3.38**	**3.48**	**N.A.**	299	N.A.	N.A.	N.A.

$T_{i,simu}$, for the associated model-generated transmission value, for those specific measured wavelengths for which the glass substrate used is reasonably transparent. The adopted FoM function in order to be minimized is really a hundred times the root-mean-square error (RMSE), corresponding to the existing differences between the as-measured and calculated transmittance data; i.e., the square root of the average of the squared transmittance differences, or residues. In the created 'AdjustTransIS Toolbox', the minimizing routine employed, as mentioned before, was the Nelder–Mead (downhill) simplex algorithm, already implemented as a particular Matlab function. It ought to be pointed out that this is a non-linear direct-search method, incorporated into the software package Matlab (R2022a) by its 'fmnsearch' function, and it was chosen in order to be able to find the minimum of an unconstrained multivariable function.

5. Influence of the finite width of the energy bands: Refining the single-oscillator model

We shall next try to determine the influence of the non-zero width of the energy band when the photon energy, E, is not very small in comparison with the optical band gap, E_{opt}. It has to be noted that the reasonably anticipated improvement of Eq. (2) will be necessarily small, but it can be fortunately measured by employing a highly-sensitive UV–Vis-NIR spectrophotometer. However, the information found upon the width of the electronic bands of the semiconductor, Δ_{eff}, even though very valuable, will only be an estimate, albeit a quite reasonable one, as it will be shown. We can now carry out some convenient simplifications that will reduce the complexity of the obtained mathematical expressions, which would just obscure the physical consequences of the existing non-zero bandwidth.

Particularly, we can assume square-shaped energy bands, therefore, having a constant density of states (DOS) from the bottom up to the top of each energy band. So, the value of the Δ_{eff}-parameter that we estimate by the model fitting shall be called 'effective width' of the electronic bands. On the other hand, we consider in this derivation that the width of the valence (bonding) and conduction (anti-bonding) energy bands are equal to each other, and that is precisely what actually happens in our case of H-free *a*-Si with just a pure sp^3 Si–Si bonding, as in unhydrogenated *a*-Si [37]. We will finally perform a new approximation concerning the transition matrix elements between the states of each energy band. At first, we have to determine the total sum of all the corresponding dipole–dipole matrix elements, between each particular energy level of the valence band and each particular energy level of the conduction band [34]. In addition, within the framework of the sp^3 tight-binding theory [38], the electronic quantum states in the energy bands are expressed as linear combinations of $|ss\rangle$ and $|ps\rangle$ eigenstates (or eigenfunctions) of the Hamilton operator, ranging from a pure $|ss\rangle$ electron state to a pure $|ps\rangle$ electron state, from the very bottom to the very top of both the valence and conduction bands, as shown in Fig. 3(a). An additional rough, but nevertheless suitable simplification, is added, that is, to only take into account as non-zero matrix elements those associated with the electronic transitions occurring just between 'symmetric' quantum states. Those two particular symmetric quantum states are the following: one state at an energy distance ξ (upward), from the very bottom of the conduction band, and the other state at exactly the same energy distance ξ (but downward, in this other case), from the very top of the valence band.

Regarding all the above-indicated simplifying steps, it should be pointed out that within the tight-binding model, in order to calculate the sum of all the transition matrix elements of the dipole–dipole operator, DD_{vc}, between the energy levels of the bonding band and those energy levels belonging to the anti-bonding band, we ought to label the quantum states conveniently. In the physics-based framework that is being employed in this work, it is now defined a set of two angle parameters, ϕ_{vs} and ϕ_{cs}, respectively, for labeling the quantum states, using the *bra–ket* notation, or Dirac notation:

$$|vs\rangle = \cos\phi_{vs}|ss\rangle + \sin\phi_{vs}|ps\rangle, \tag{5}$$

$$|cs\rangle = \sin\phi_{cs}|ss\rangle + \cos\phi_{cs}|ps\rangle. \tag{6}$$

The valence angle variable, ϕ_{vs}, varies from 0 to $\pi/2$ radian, from the bottom up to the top of the valence band (upward direction). And, in the same manner, the conduction angle variable, ϕ_{cs}, varies from 0 to $\pi/2$ radian, from the top down to the bottom (downward direction). This way of particular labeling of the quantum states satisfies the pure *s* and pure *p* character of the energy-band edges, as shown in Fig. 3(a). Considering next that the transition matrix elements of the dipole–dipole operator, DD_{vc}, are non-zero exclusively between $|ss\rangle$ and $|ps\rangle$ states, we obtain that:

$$\left|\langle vs|DD_{vc}|cs\rangle\right|^2 = \cos^2(\phi_{vs}-\phi_{cs})\left|\langle ss|DD_{vc}|ps\rangle\right|^2. \tag{7}$$

Thus, a pronounced maximum of the transition matrix elements is found for the particular case of $\phi_{vs} = \phi_{cs}$, i.e., between those quantum states that were previously designated as symmetric states. Finally, we carry out another very convenient simplification in order to ease the algebraic expressions, but without modifying the physics of the present system. If we substitute $\cos^2(\phi_{vs}-\phi_{cs})$ by $\delta(\phi_{vs}-\phi_{cs})$, that is, the Dirac delta function or, δ distribution, the existing double sum of all the transition matrix elements between the valence and conduction bands, now transforms to just a single sum. Thus, we can derive the following integral equation:

$$n^2(E) = 1 + (n^2(0)-1)\frac{1}{2\Delta_{eff}}\int_{E_{M,Sol}-\Delta_{eff}}^{E_{M,Sol}+\Delta_{eff}} \frac{\xi^2}{\xi^2-E^2}\,d\xi. \tag{8}$$

This expression can be interpreted from the physical point of view, as follows: The electronic dielectric constant of a two-energy-level system, with Eq. (2) as its characteristic equation, is now substituted by the average of all the single-oscillator-system values for each pair of the symmetrical quantum states of the valence and conduction bands, as has been previously expressed in Eq. (2). Since it can be written

$$\int_{E_{M,Sol}-\Delta_{eff}}^{E_{M,Sol}+\Delta_{eff}} \frac{\xi^2}{\xi^2-E^2}\,d\xi = \xi - E\tanh^{-1}\frac{\xi}{E}\Bigg|_{E_{M,Sol}-\Delta_{eff}}^{E_{M,Sol}+\Delta_{eff}}$$
$$= \xi - E\frac{1}{2}\ln\frac{E-\xi}{E+\xi}\Bigg|_{E_{M,Sol}-\Delta_{eff}}^{E_{M,Sol}+\Delta_{eff}}, \tag{9}$$

the integration of Eq. (8) results in the following relationship:

$$n^2(E) = 1 + \chi(E) =$$
$$1 + (n^2(0)-1)\left[1 + \frac{E}{4\Delta_{eff}}\ln\left(\frac{E_{M,Sol}^2 - (\Delta_{eff}-E)^2}{E_{M,Sol}^2 - (\Delta_{eff}+E)^2}\right)\right], \tag{10}$$

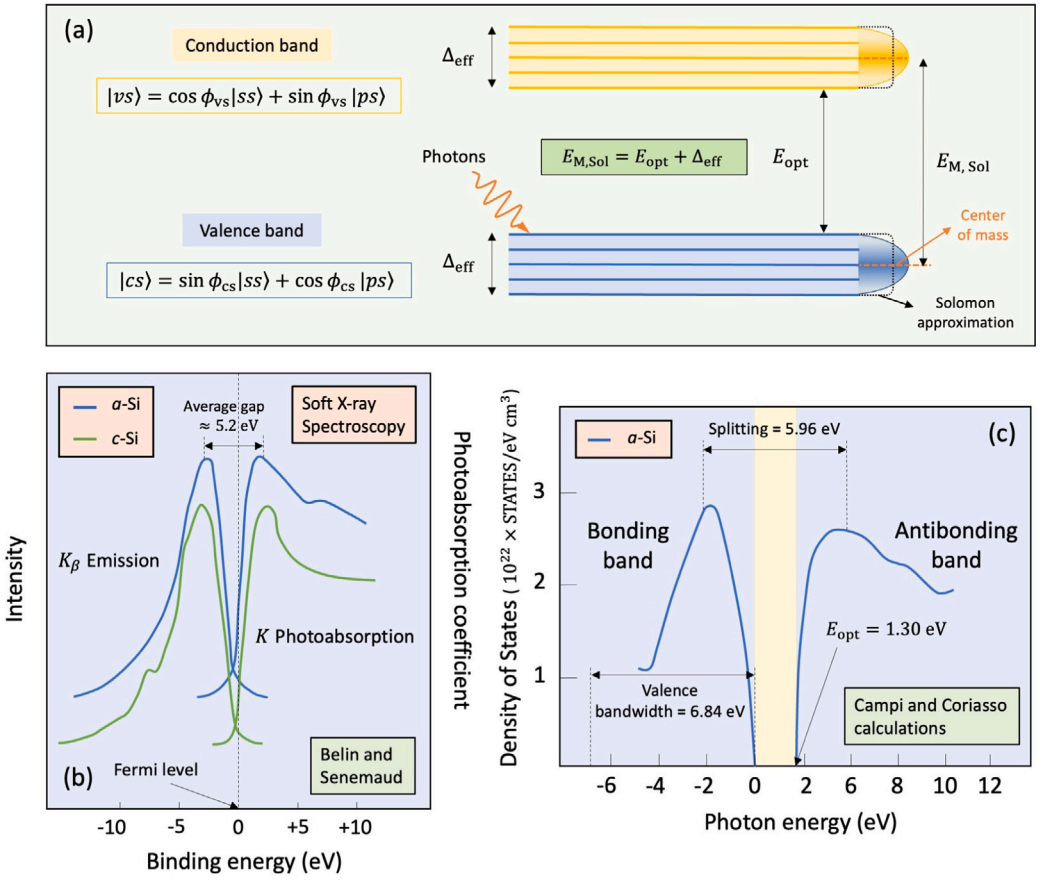

Fig. 3. (a) Schematic diagram of the energy-band structure of *a*-Si. This conveniently simplified picture is fully described by only three energy parameters: the Tauc optical gap, E_{opt}, the Solomon average gap, $E_{M,Sol}$, and the corresponding effective bandwidth, Δ_{eff}. As pointed out in the text, the bottom and top of each electronic band are *s* type and *p* type, respectively, due to the sp^3 nature of the existing Si–Si chemical bonds. (b) Si K_β emission and Si K photoabsorption from *a*-Si material [39]. (c) The valence- and conduction-energy-band density-of-states of *a*-Si as determined in [26,40]. The energy intervals corresponding to the Campi and Coriasso model parameters, this is, the splitting of 5.96 eV, the valence bandwidth of the 6.84 eV, and the calculated value of E_{opt} of 1.30 eV, have been explicitly shown.

where $\chi(E)$ is the linear susceptibility. In order to be able to contrast this new equation with Eq. (2), we next consider that

$$\frac{\chi(0)}{\chi(E)} = \frac{n^2(0)-1}{n^2(E)-1} = \frac{1}{1+\dfrac{E}{4\Delta_{eff}}\ln\left(\dfrac{E^2_{M,Sol}-(\Delta_{eff}-E)^2}{E^2_{M,Sol}-(\Delta_{eff}+E)^2}\right)}, \tag{11}$$

and use the Taylor expansion,

$$\frac{\chi(0)}{\chi(E)} = 1-\left(\frac{E}{E_{corr}}\right)^2-\beta\left(\frac{E}{E_{corr}}\right)^4-\gamma\left(\frac{E}{E_{corr}}\right)^6-\ldots, \tag{12}$$

where

$$E^2_{corr} = E^2_{M,Sol} - \Delta^2_{eff},$$

$$\beta = \frac{4}{3}\frac{\Delta^2_{eff}}{E^2_{corr}}$$

and

$$\gamma = \frac{4\Delta^2_{eff}}{3E^2_{corr}}\left(\frac{5E^2_{corr}+12\Delta^2_{eff}}{5E^2_{corr}}\right) = \beta\left(1+\frac{9}{5}\beta\right).$$

So that, truncating beyond the fourth-order term, we obtain

$$n^2(E) = 1+(n^2(0)-1)\frac{1}{1-(E/E_{corr})^2-\beta(E/E_{corr})^4}. \tag{13}$$

We can easily confirm that Eq. (13) is fully consistent with the single-effective-oscillator formula, Eq. (2), when the effective bandwidth, Δ_{eff}, equals zero, since they both, as it should be expected, totally coincide. And it is also deduced that $E_{corr} \equiv E_{M,WD}$, and hence it is derived the following interrelationship between the Solomon average gap, $E_{M,Sol}$, and the Wemple–DiDomenico average gap, $E_{M,WD}$:

$$E^2_{M,Sol} = E^2_{M,WD} + \Delta^2_{eff}, \tag{14}$$

or equivalently expressed,

$$E_{M,Sol} = E_{M,WD} \oplus \Delta_{eff}, \tag{15}$$

where $\oplus$ denotes the Pythagorean addition, also named addition in quadrature.

It has to be stressed that the previous Solomon normal-dispersion model for the refractive index is only valid for the photon-energy range where it is verified that $E < E_{opt}$, as it should be. In order to unambiguously demonstrate that, we now substitute the previous relationship $E_{M,Sol} = E_{opt} + \Delta_{eff}$ (see Fig. 3(a)), into Eq. (10). Moreover, we then get an alternative expression of the $n(E)$-dependence in a convenient and clarifying form:

$$n^2(E) = 1+(n^2(0)-1)\times \left[1+\frac{E}{4(E_{M,Sol}-E_{opt})}\ln\frac{[2E_{M,Sol}-(E_{opt}+E)](E_{opt}+E)}{[2E_{M,Sol}-(E_{opt}-E)](E_{opt}-E)}\right], \tag{16}$$

where the revealing appearance in the denominator of the logarithmic term of the difference between the band-gap energy and the photon energy, $E_{opt} - E$, necessarily obligates to be considered only the sub-band-gap spectral region, where $E < E_{opt}$ when applying the Solomon approach, which is, as said before, an exclusively *normal-dispersion* model.

If we perform a *seven*-parameter fit to Eq. (16), we would, in theory, be able to compute the values of the *three* free geometrical and

Table 2
Optical properties, together with the void volume fractions of the three *a*-Si specimens under study. The parameter $n(0)$ is the Solomon static refractive index, $E_{M,Sol}$ and Δ_{eff} are the Solomon energy-band parameters, E_{opt} is the Tauc gap, E_U is the Urbach energy, $\bar{d}$ is the average film thickness, Δd is the thickness variation, FoM is the value of the figure of merit, and f_{void}^{Bru} and f_{void}^{MG} are the void volume fractions, calculated based upon the BEMA and MG approaches, respectively.

a-Si specimen ID	$n(0)$	$E_{M,Sol}$ (eV)	E_{opt} (meV)	Δ_{eff} (eV)	E_U (meV)	$\bar{d}$ (or d) (nm)	Δd (nm)	FoM	f_{void}^{Bru}	f_{void}^{MG}
#1	3.11	**5.57**	**1.37**	**4.20**	243	1123	0	0.673	0.22	0.24
#2	3.16	**5.41**	**1.38**	**4.03**	258	769	25	0.455	0.21	0.22
#3	3.34	**5.37**	**1.32**	**4.05**	230	1174	0	0.849	0.14	0.15
device-grade *a*-Si:H [10]	3.44	**4.66**	**1.90**	**2.75**	N.A.	299	N.A.	N.A.	N.A.	N.A.

optical parameters $\bar{d}$, Δd and $n(0)$, and those *two* corresponding to the energy-band parameters, $E_{M,Sol}$ and Δ_{eff}, respectively. We would also get the values of the *two* additional absorption parameters belonging to the Urbach absorption tail, α_0 and E_U, respectively. However the reality is that only *five* of the obtained values of free parameters, $\bar{d}$, Δd, $n(0)$, α_0, and E_U, respectively, are physically reasonable. In fact, they are almost coincident with the values of these *five* parameters previously obtained with the fit corresponding to the other particular combination of the WD model for $n(E)$, and the Urbach rule for $\alpha(E)$. However, the fitted values of the $E_{M,Sol}$ and Δ_{eff} are both unrealistic and unphysical ones, the computed bandwidth being very small, close to zero, and even in some cases being unphysical negative values. This is in sharp contradiction with what has been reported by Solomon [10] when determining the electronic-band structure of his case study of the device-grade *a*-Si:H material, as well as a series of *a*-$Si_{1-x}C_x$: H alloys. It should be additionally indicated that he did *not* take into account in his model fit the existing below-band-gap weak absorption, associated to the mentioned Urbach–Martienssen tails, and he simply considered the material to be absolutely transparent, with the very rough assumption of $\alpha = k = 0$.

5.1. Using the independent tauc band-gap determination based upon the absorption-coefficient data

We do propose a new and necessary step, which consists in modifying the previous fit to a *six* free parameter fit, as explained below, offering physically-reasonable highly-accurate results. Additionally, from Fig. 3(a), it can be recalled that the three band parameters E_{opt}, $E_{M,Sol}$ and Δ_{eff}, respectively, are correlated by the equation $E_{M,Sol} = E_{opt} + \Delta_{eff}$. As the Tauc optical bandgap, E_{opt}, can be independently calculated from the absorption coefficient, α, of above-band-gap light, $E_{M,Sol}$ and Δ_{eff} (or the two intermediate parameters E_{corr} and β from Eq. (12)), can be instead interpreted just as a single free fitting parameter. By Eq. (16), and introducing in it the relationship $\Delta_{eff} = E_{M,Sol} - E_{opt}$, the fitting is finally modified to the aforementioned *six*-parameter fitting.

Concerning the determination of the optical gap, it should be said that some authors avoid the use of the Tauc plot, which requires an, up to a point, rather ill-defined extrapolation, the Tauc extrapolation, subject sometimes to relatively large statistical errors. And instead, evaluate the energy, E_{04}, at which the absorption coefficient equals the value of α of $10^4\,cm^{-1}$. This energy is about 0.15 eV higher than the actual Tauc gap, E_{opt}, for *a*-Si. We have, in fact, confirmed in our work this particular difference between the two gap parameters E_{04} and E_{opt}, respectively. And they generally state that this energy difference is truly insignificant for the discussion of the experimental results. However, in our present approach, we have made use of the well-known Tauc extrapolation, as the majority of the researchers in the field. Let us now recall the Tauc expression for the fundamental absorption edge. According to Tauc et al. [41,42], for $\alpha \gtrsim 10^4\,cm^{-1}$ (the Tauc's region), it is obeyed that:

$$\sqrt{\alpha E} = C_{Tauc}(E - E_{opt}). \tag{17}$$

This is the Tauc law, employed in order to calculate the Tauc optical gap, E_{opt}, and the Tauc slope, C_{Tauc}, from the previously-determined values of α. See all details in Fig. 4.

5.2. Obtaining the optical constants by using the novel Solomon–Urbach approach

We have made use of the proposed optical characterization method based upon the Solomon–Urbach model by initially fixing for it the independently-determined value of the Tauc gap E_{opt}, belonging to the hydrogen-free *a*-Si specimens #1 and #2 of 1.37 eV and 1.38 eV, respectively. The values of the six fitting parameters $\bar{d}$, Δd, $n(0)$, $E_{M,Sol}$ (or equivalently Δ_{eff}), α_0 and E_U, respectively, are next computed, and presented in Fig. 5 and Table 2, together with their respective low values of the figure of merit, FoM, of 0.673 and 0.849. See the two Matlab GUIs corresponding to the two *a*-Si specimens #1 (a), and #3 (b), respectively, displayed in Fig. 5. We thus confirm the consistency and accuracy of the novel procedure based upon the devised Solomon–Urbach model. It has to be also mentioned that the values of some FP-interference order numbers are shown in Fig. 5, in order to enrich the present analysis of the transmission curves.

Continuing with the discussion of the optical properties, in particular the complex refractive index, $\boldsymbol{n} = n - ik$, of *a*-Si layers, it is observed in Fig. 6 that in the range of low photon energy, n is an increasing function of the photon energy (i.e., $dn/dE > 0$). The optical dispersion is then called normal dispersion. For values of photon energy larger than approximately E_{opt}, the refractive index starts increasing in a *slower* fashion, instead, with increasing photon energy (i.e., $d^2n/dE^2 < 0$). And eventually the values of n commence decreasing (i.e., $dn/dE < 0$), which is then the so-called the regime of 'anomalous' dispersion, which is certainly not seen the present case. It must be noted that from the Kramers–Kronig bidirectional mathematical relations, the refractive index has to be necessarily correlated to the existing optical absorptions of the *a*-Si films under study, clearly shown by the observed behavior of the extinction coefficient, k (see Fig. 6).

6. Alternate calculation of the refractive index and film thickness by Swanepoel model-free graphical method

According to the Swanepoel model-free envelope method [2], based upon the approach devised initially by Manifacier et al. [1], of constructing the two continuous envelope functions around the FP interference maxima and minima, a first (crude) value of the refractive index of the layer, n_1, in the spectral regions of weak and medium absorption, is calculated by the following expression:

$$n_1(\lambda) = \sqrt{\widehat{T}(\lambda) + \sqrt{\widehat{T}^2(\lambda) - s^2(\lambda)}}, \tag{18}$$

where

$$\widehat{T}(\lambda) = 2s(\lambda)\frac{T_+(\lambda) - T_-(\lambda)}{T_+(\lambda)T_-(\lambda)} + \frac{s^2(\lambda)+1}{2}.$$

Here T_+ and T_- are really the upper and lower *tangent* envelopes of the normal-incidence transmission spectrum, respectively, rather than the envelopes of the peaks and valleys of the transmittance curve. Moreover, the values of the refractive index, $s(\lambda)$, of the transparent glass substrate, have been determined from the transmission spectrum

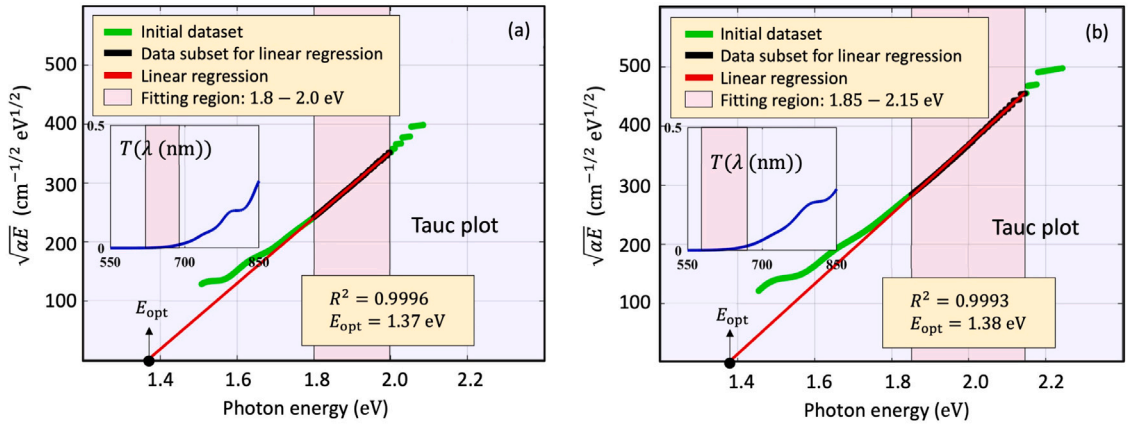

Fig. 4. The Tauc optical band gap determined by the Tauc plot. We show the Tauc linear extrapolations for the non-hydrogenated *a*-Si data, belonging to the *a*-Si specimens #1 (a) and #2 (b), respectively. The extrapolated Tauc gaps are conveniently marked with arrows. (Adapted from [25] by E. Marquez et al.).

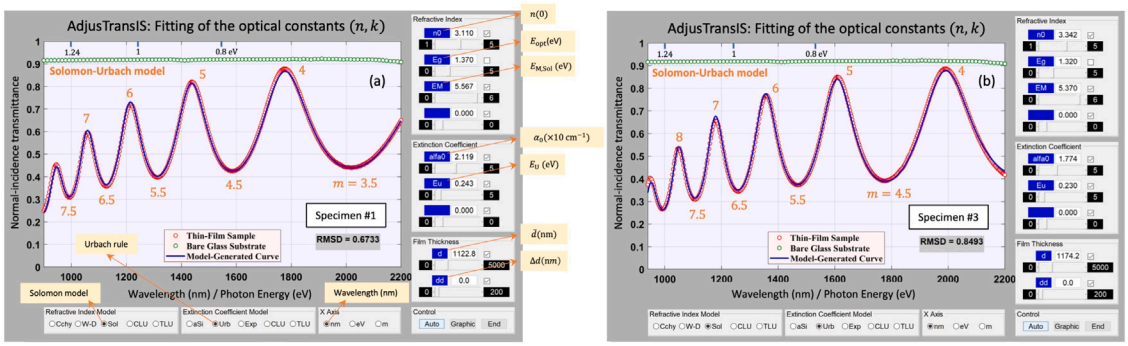

Fig. 5. Transmission spectrum for *a*-Si specimen #1 (a), and also that for *a*-Si specimen #3 (b). Matlab graphical-user-interface (GUI, or main window) screen for the accurate optical characterization of wedge-shaped thin layers of amorphous semiconductor materials, belonging to the devised Matlab-coded computer program, 'AdjusTransIS Toolbox'. Appropriate checkboxes and radio buttons are used in this GUI for the quick and accurate transmission-data analysis carried out in the present work, based in this particular case upon the proposed Solomon–Urbach dispersion model. Moreover, the values of some FP-interference order number are indicated in the figure. The very low computed values of FoM are also inserted into the figure, for the two specimens #1 and #3, respectively.

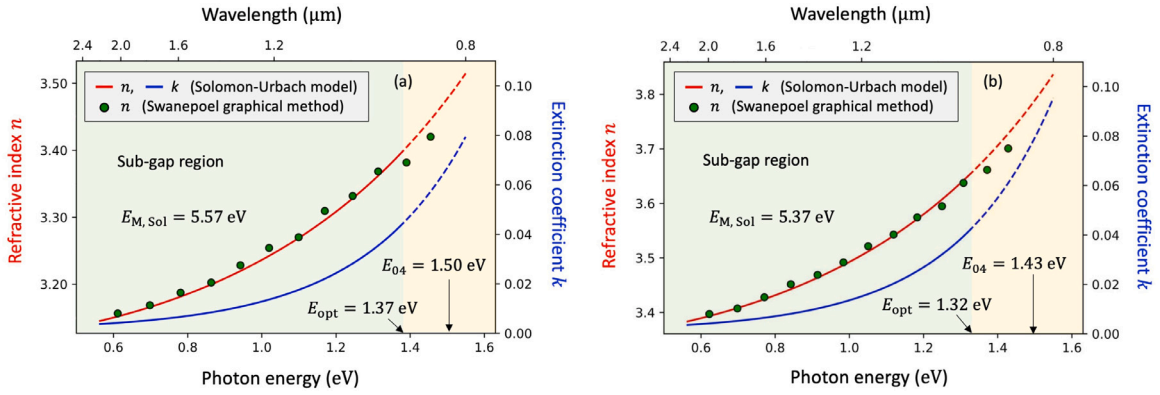

Fig. 6. Plots of the refractive index, n, and extinction coefficient, k, belonging to the *a*-Si specimen #1 (a), and the *a*-Si specimen #3 (b). Best fit associated to the transmission data corresponding to the investigated *a*-Si thin films, using the newly proposed Solomon–Urbach normal-dispersion model. Also shown in the figure, the values of n directly determined by the model-free graphical envelope method suggested by Swanepoel.

of the uncoated glass substrate, T_s, by employing the well-known formula for a thick slab:

$$s(\lambda) = \frac{1}{T_s(\lambda)} + \sqrt{\frac{1}{T_s^2(\lambda)} - 1}. \tag{19}$$

On the other hand, it is taken into account the basic spectrophotometric equation associated to the FP-interference pattern:

$$2n(\lambda_{tan})d = m\lambda_{tan}, \tag{20}$$

where the interference order number, m, is an integer for the top tangent points and half-integer for the bottom tangent points. By using the 'Swanepoel graphical method' [2], based upon Eq. (20). which can be appropriately re-written to that end, as follows,

$$\frac{\ell}{2} = 2d\frac{n(\lambda_{tan})}{\lambda_{tan}} - m_1, \tag{21}$$

where $\ell = 0, 1, 2, \ldots$, and m_1 is the first interference order, the exact values of m and also the highly-accurate value of d have been determined.

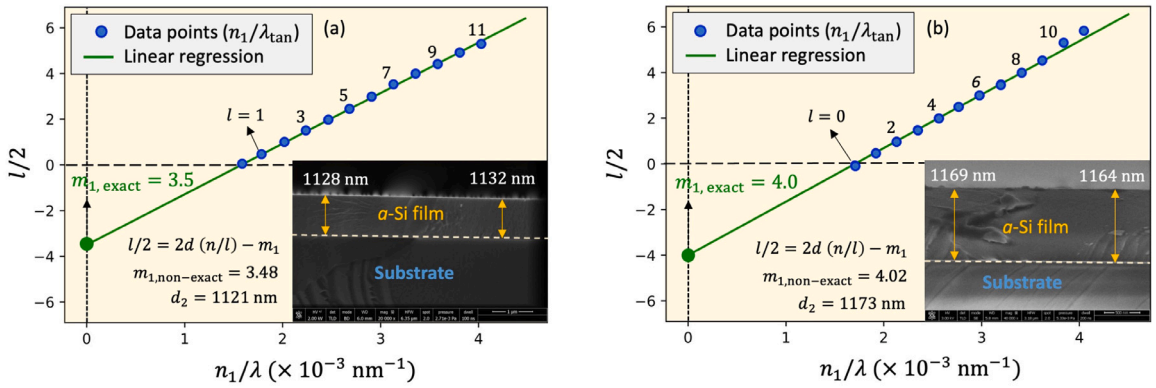

Fig. 7. Plots of $l/2$ versus n/λ (Swanepoel model-free graphical envelope method), in order to determine the layer thickness, d_{graph}, and the first exact FP-interference order number, $m_{1,exact}$, for the *a*-Si specimen #1 (a) and #3 (b). The cross-sectional SEM micrographs for both samples are also shown in this figure, as insets. The two directly-measured values of film thickness, d_{SEM}, are marked in the insets.

So, by plotting $\ell/2$ vs. $n(\lambda_{tan})/\lambda_{tan}$ yields a straight line, with slope $2d$ and cut-off on the vertical axis, m_1. Fig. 7 displays this particular graph for the specimens #1 and #3. The final calculated values of d are 1123 nm and 1174 nm, respectively, and those of $m_{1,exact}$ are 3.5 and 4.0, respectively. It has to be emphasized that two linear fit has been performed.

By the first one, the slope, $2d_1$, and the non-exact-value of m_1, $m_{1,non\text{-}exact}$, are reasonably estimated. And by the second one, with the exact value of m_1 fixed following the nearest-integer or half-integer value as clearly shown in Fig. 7, the final value of the slope, $2d_2$, is then accurately determined (see Table 3).

6.1. On the newly-introduced table associated with the cross-checking graphical envelope method

Regarding the rest of the content of the tables, let us point out the following: The corresponding data when choosing from 2 up to 12 points in the linear fitting are listed. The columns $2d_1$ and $m_{1,non\text{-}exact}$ are associated to a linear fit in both coefficients (the slope and intercept form). Then, the lowest integer or half-integer order m_1 is *forced* to its exact right position (integer for a maximum and half an integer for a minimum). The following column readjusts the final, more accurate value of the slope, $2d_2$. The last column is the proposed measure for the error: namely, the ratio RMSE/N_{points}, in order to get a very conveniently normalized value, is used in order to compare the procedures involving different straight lines in this graphical-method table. The plots of Fig. 7 are obtained by using the data found with the values of N_{points} of 11 and 6, respectively. See all the details in Table 3. The final, more accurate values for the refractive index, n_2, after applying the graphical envelope method, and making use of Eq. (20), are also finally presented in Table 3 and Fig. 6.

7. Void-volume-fraction calculation: Bruggeman and Maxwell-Garnet effective medium approximations

We can now extract valuable information from the value of the static refractive index, $n(0)$, clearly related to the porosity of the layer. Hence, a calculation of the void volume fraction, f_{void}, for the *a*-Si thin films under study, by employing the self-consistent Bruggeman effective medium approximation (BEMA) [43], and the values of the static refractive index, $n(0)$, determined by the Solomon–Urbach model fit, is next performed.

Following this particular BEMA theory, a combination of various materials can be treated as a homogeneous medium, having an effective complex dielectric constant, ε_{eff}, that can be found from their individual complex dielectric constants, ε_i's, and their associated volume fractions, f_i's, whereas it is verified the condition: $\sum_i f_i = 1$. According to the BEMA approach, for a composite material made up of several *i*-constituent components, the relationship to be obeyed is the following:

$$\sum_i f_i \left(\frac{\varepsilon_i - \varepsilon_{eff}}{\varepsilon_i + 2\varepsilon_{eff}} \right) = 0. \tag{22}$$

By making use of the basic equation between the complex dielectric constant and the complex refractive index, $\varepsilon = \boldsymbol{n}^2$, and by taking into consideration the two existing constituent components of our *a*-Si thin layer, the solid material and the embedded voids (pores), whose respective volume fractions are, $1 - f_{void}^{Bru}$ (for the dense, or pore- or void-free unhydrogenated *a*-Si), and f_{void}^{Bru} (for the air-filled voids or pores), together with setting $n_{eff}(0) \equiv n_{porous}(0)$, we can finally re-write Eq. (22), as follows,

$$\left(1 - f_{void}^{Bru}\right) \left(\frac{n_{dense}^2(0) - n_{porous}^2(0)}{n_{dense}^2(0) + 2n_{porous}^2(0)} \right) + f_{void}^{Bru} \left(\frac{1 - n_{porous}^2(0)}{1 + 2n_{porous}^2(0)} \right) = 0. \tag{23}$$

Therefore, by solving for f_{void}, we reach the final, closed-form expression:

$$f_{void}^{Bru} = \frac{(1 + 2n_{porous}^2(0))n_{dense}^2(0) - n_{porous}^2(0)}{3n_{porous}^2(0)(n_{dense}^2(0) - 1)}. \tag{24}$$

The necessary value of the refractive index in order to calculate the value of f_{void}^{Bru}, i.e., the value of $n(0)$ for the dense, self-implanted, fully *a*-Si, $n_{dense} = 3.697$ [44,45], is now introduced in the above formula, for f_{void}^{Bru}, Eq. (24). On the other hand, the value of the refractive index of air, $n_{air} = 1$, was previously inserted in Eq. (23). The obtained values of the BEMA-based void volume fraction, f_{void}^{Bru}, are listed in Table 2.

There is another very popular mixture rule for dispersed dielectric spheres, such as the case of the air pores present in our non-hydrogenated *a*-Si specimens, and embedded in a continuous dielectric matrix, that works certainly very well for volume fractions up to a specific value of about 20 %, as it has also been corroborated in this investigation, called the Maxwell-Garnet formula [43]:

$$\frac{n_{porous}^2(0) - n_{dense}^2(0)}{n_{porous}^2(0) + 2n_{dense}^2(0)} = f_{void}^{MG} \left(\frac{1 - n_{dense}^2(0)}{1 + 2n_{dense}^2(0)} \right). \tag{25}$$

Then, by solving for the void volume fraction, f_{void}^{MG}, we get:

$$f_{void}^{MG} = \left(\frac{n_{porous}^2(0) - n_{dense}^2(0)}{1 - n_{dense}^2(0)} \right) \left(\frac{1 + 2n_{dense}^2(0)}{n_{porous}^2(0) + 2n_{dense}^2(0)} \right). \tag{26}$$

This Maxwell-Garnet (MG) relationship can accurately predict the effective dielectric constant of the H-free fully *a*-Si material that have, nevertheless, dispersed pores. Therefore, as proved in this work, the MG formula is particularly useful for the calculation of the value of porosity of the investigated *a*-Si films. The calculated values of the parameter f_{void}^{MG} are also listed in Table 2.

Table 3
Swanepoel optical-characterization graphical method for the two representative *a*-Si specimens #1 and #3, respectively. Values of the optical and geometrical parameters λ_{tan}, T_+, T_-, s, n_1, N_{points}, $2d_1$, $m_{1,non\text{-}exact}$, $2d_2$, $m_{1,exact}$, RMSE/N_{points}, m_{exact} and n_2, obtained from their respective normal-incident transmission spectra, by using the model-free (direct) graphical envelope method. The meaning of all the symbols indicated are described in the text.

λ_{tan} (nm)	T_+	T_-	s	n_1	N_{points}	$2d_1$ (nm)	$m_{1,non\text{-}exact}$	$2d_2$ (nm)	$m_{1,exact}$	RMSE/N_{points} ($\times 10^{-7}$)	m_{exact}	n_2
a-Si specimen #1			[$d_{2,graph}$ = 1121 nm, $m_{1,graph}$ = 3.5]									
2028	0.8748	0.4395	1.514	3.149	N.A.	N.A.	N.A.	N.A.	N.A.	N.A.	**3.5**	**3.207**
1776	0.8747	0.4342	1.511	3.173	2	2138	3.32	2243	3.5	28.0	**4.0**	**3.210**
1588	0.8542	0.4258	1.511	3.190	3	2192	3.41	2243	3.5	16.9	**4.5**	**3.229**
1436	0.8192	0.4146	1.523	3.217	4	2188	3.40	2239	3.5	16.0	**5.0**	**3.244**
1316	0.7704	0.4000	1.516	3.220	5	2230	3.48	2242	3.5	13.4	**5.5**	**3.270**
1216	0.7118	0.3782	1.519	3.259	6	2230	3.48	2241	3.5	10.4	**6.0**	**3.296**
1128	0.6463	0.3510	1.521	3.320	7	2189	3.40	2233	3.5	21.8	**6.5**	**3.313**
1060	0.5826	0.3237	1.523	3.388	8	2153	3.32	2224	3.5	30.3	**7.0**	**3.353**
996	0.5077	0.2940	1.526	3.445	9	2118	3.25	2213	3.5	38.4	**7.5**	**3.375**
944	0.4355	0.2714	1.529	3.410	10	2142	3.30	2213	3.5	32.8	**8.0**	**3.412**
892	0.3526	0.2428	1.531	3.315	11	2211	3.46	2226	3.5	42.1	**8.5**	**3.426**
852	0.2806	0.2051	1.522	3.331	12	2266	3.58	2238	3.5	47.4	**9.0**	**3.465**
a-Si specimen #3			[$d_{2,graph}$ = 1173 nm, $m_{1,graph}$ = 4.0]									
1992	0.8865	0.3917	1.511	3.421	N.A.	N.A.	N.A.	N.A.	N.A.	N.A.	**4.0**	**3.397**
1776	0.8729	0.3915	1.511	3.406	2	2494	4.28	2339	4.0	33.4	**4.5**	**3.407**
1608	0.8498	0.3840	1.511	3.423	3	2431	4.17	2343	4.0	22.8	**5.0**	**3.428**
1472	0.8145	0.3724	1.516	3.456	4	2377	4.07	2343	4.0	14.8	**5.5**	**3.452**
1356	0.7681	0.3592	1.513	3.475	5	2358	4.03	2342	4.0	10.6	**6.0**	**3.469**
1260	0.7137	0.3444	1.518	3.498	6	2349	4.02	2342	4.0	8.12	**6.5**	**3.492**
1180	0.6558	0.3281	1.520	3.519	7	2355	4.03	2343	4.0	7.23	**7.0**	**3.522**
1108	0.5954	0.3092	1.521	3.548	8	2349	4.02	2343	4.0	5.97	**7.5**	**3.543**
1048	0.5348	0.2899	1.523	3.573	9	2352	4.02	2344	4.0	5.32	**8.0**	**3.574**
992	0.4655	0.2665	1.526	3.597	10	2350	4.02	2344	4.0	4.55	**8.5**	**3.595**
948	0.4003	0.2416	1.529	3.632	11	2352	4.02	2345	4.0	4.45	**9.0**	**3.638**
904	0.3218	0.2096	1.530	3.654	12	2355	4.03	2346	4.0	4.48	**9.5**	**3.661**
868	0.2473	0.1781	1.533	3.578	13	2406	4.18	2357	4.0	28.1	**10.0**	**3.701**

The range of values of the porosity for the specific RF-magnetron sputtering deposition conditions used in this research, with a particular range of Ar-working pressure of around 2.4-4.4 Pa, was approximately 14-22 %. The values of porosity found by the two EMAs employed are very consistent with those values of porosity recently reported by Karabacak and Demirkan [17,18], as large as around 30 %, corresponding, in their case to a measured value of the film mass density of about 1.64 g cm^{-3}.

8. Comparison with the direct band-structure determination: Reported soft X-ray spectroscopy measurements

A comparison and subsequent validation of our obtained value of the average gap, $E_{M,Sol}$, with direct measurements of the energy-band structure, made by using the soft X-ray spectroscopy (SXS) technique and reported by Belin and Senemaud [39], is now undertaken. This specific technique does need ultra-high vacuum equipment and a specific manner of preparing the specimen. However, in spite of its intrinsic complexity, it gives the possibility of providing direct information regarding the density of states of the material. In particular, it was reported a value of the peak-to-peak energy, E_{pp}, associated with the valence and conduction bands (i.e., the bonding/anti-bonding splitting), of approximately 5.2 eV (see Fig. 3(b)).

It is obliged to say at this point that a complete quantitative agreement between the values of the energy parameters $E_{M,Sol}$ and E_{pp} must not be expected because the peak of the density of states in the valence and conduction band does not correspond exactly to the weighted average used in the determination of the average gap, within the two-band model. Instead, this takes into account not only the density of states, but also the respective matrix elements of the electronic transition probabilities.

Nevertheless, the obtained values of the band parameters, $E_{M,Sol}$ and E_{pp}, respectively, in the energy range of 5.0-6.0 eV (see the obtained values in Table 2), are surprisingly close to each other, taking into consideration the whole set of simplifying steps taken in order to eventually reach Eq. (16). And that closeness found between $E_{M,Sol}$ and E_{pp} is clearly much greater than that corresponding to the case of the WD single-effective-oscillator model, thus justifying the usefulness of the proposed refractive-index correction.

Furthermore, it has been reported by Campi and Coriasso [40,46], the calculated values of the bonding/anti-bonding splitting and the valence bandwidth of 5.96 eV and 6.89 eV, respectively (see Fig. 3(c)). They have been determined assuming the tight-binding approximation, and these two calculated values of the two band parameters are certainly consistent with what was determined by the present Solomon–Urbach dispersion-model fit.

9. Concluding remarks

We have unambiguously demonstrated that the in-depth analysis of exclusively the normal-incidence transmission spectrum of the below-band-gap light permits the reasonably accurate calculation of the main parameters of the band structure of an amorphous semiconductor film. We have used to that end a universal transmission formula previously derived by the authors, which can be applied even to strongly-wedge-shaped layers. By doing that, we have been able to determine the average film thickness, $\bar{d}$, and film thickness non-uniformity, Δd, together with the optical constants, refractive index, n, and extinction coefficient, k, respectively, of the semiconductor material, as a function of the photon energy, E. We have also calculated the value of the pre-exponential factor of the Urbach equation, α_0, and that of the Urbach-energy parameter, E_U. The novel Solomon–Urbach approach presented in this work has been very successfully applied to a series of non-hydrogenated *a*-Si specimens, grown by radio-frequency magnetron sputtering deposition, onto room-temperature glass substrates, with slightly different Ar working pressures.

Last but not the least, it must be again emphasized that the aforementioned values of the energy-band parameters, $E_{M,Sol}$ and E_{pp}, respectively, are indeed surprisingly near each other, if we consider

the various assumptions previously introduced in order to finally derive the very convenient, Eq. (16). And this particular expression of the refractive-index dispersion, $n(E)$, is the base of our proposed Solomon–Urbach approach.

CRediT authorship contribution statement

M. Ballester: Conceptualization, Software, Investigation, Visualization. **A.P. Márquez:** Software, Validation, Writing – original draft. **C. García-Vázquez:** Validation, Writing – review and editing. **J.M. Díaz:** Validation, Writing – review and editing. **E. Blanco:** Resources, Visualization. **D. Minkov:** Validation. **S.M. Fernández-Ruano:** Data curation, Funding acquisition. **F. Willomitzer:** Supervision, Project administration. **O. Cossairt:** Supervision, Project administration. **E. Márquez:** Conceptualization, Methodology, Formal analysis, Investigation, Resources, Writing – original draft, Supervision, Project administration, Funding acquisition.

Declaration of competing interest

The authors declare that they have no known competing financial interests or personal relationships that could have appeared to influence the work reported in this paper.

Data availability

Data will be made available on request.

Acknowledgments

This research was funded by the SCALED project, Spain, grant number PID2019-109215RB-C42, provided by the Ministerio de Ciencia, Innovación *y* Universidades (Spain).

References

[1] J.C. Manifacier, J. Gasiot, J.P. Fillard, A simple method for the determination of the optical constants *n*, *k* and the thickness of a weakly absorbing thin film, J. Phys. E: Sci. Instrum. 9 (11) (1976) 1002.
[2] R. Swanepoel, Determination of the thickness and optical constants of amorphous silicon, J. Phys. E: Sci. Instrum. 16 (12) (1983) 1214.
[3] R. Swanepoel, Determination of surface roughness and optical constants of inhomogeneous amorphous silicon films, J. Phys. E: Sci. Instrum. 17 (10) (1984) 896.
[4] E. Márquez, J. Díaz, C. García-Vázquez, E. Blanco, J. Ruiz-Pérez, D. Minkov, G. Angelov, G. Gavrilov, Optical characterization of amine-solution-processed amorphous ass2 chalcogenide thin films by the use of transmission spectroscopy, J. Alloys Compd. 721 (2017) 363–373, http://dx.doi.org/10.1016/j.jallcom.2017.05.303.
[5] J.J. Ruiz-Pérez, E.M. Navarro, Optical transmittance for strongly-wedge-shaped semiconductor films: appearance of envelope-crossover points in amorphous as-based chalcogenide materials, Coatings 10 (11) (2020) 1063, http://dx.doi.org/10.3390/coatings10111063.
[6] D.A. Minkov, Calculation of the optical constants of a thin layer upon a transparent substrate from the reflection spectrum, J. Phys. D: Appl. Phys. 22 (8) (1989) 1157.
[7] C. Corrales, J.B. Ramírez-Malo, J. Fernández-Peña, P. Villares, R. Swanepoel, E. Márquez, Determining the refractive index and average thickness of AsSe semiconducting glass films from wavelength measurements only, Appl. Opt. 34 (34) (1995) 7907, http://dx.doi.org/10.1364/ao.34.007907.
[8] I. Solomon, M.P. Schmidt, H. Tran-Quoc, Selective low-power plasma decomposition of silane-methane mixtures for the preparation of methylated amorphous silicon, Phys. Rev. B 38 (14) (1988) 9895–9901, http://dx.doi.org/10.1103/physrevb.38.9895.
[9] I. Solomon, M.P. Schmidt, C. Sénémaud, M.D. Khodja, Band structure of carbonated amorphous silicon studied by optical, photoelectron, and x-ray spectroscopy, Phys. Rev. B 38 (18) (1988) 13263–13270, http://dx.doi.org/10.1103/physrevb.38.13263.
[10] I. Solomon, Band-structure determination by subgap spectroscopy in thin films of semiconductors, Phil. Mag. B 76 (3) (1997) 273–280, http://dx.doi.org/10.1080/01418639708241092.
[11] D.E. Carlson, C.R. Wronski, Amorphous silicon solar cell, Appl. Phys. Lett. 28 (11) (1976) 671–673, http://dx.doi.org/10.1063/1.88617.
[12] R.A. Street, Hydrogenated Amorphous Silicon, in: Cambridge Solid State Science Series, Cambridge University Press, 1991, http://dx.doi.org/10.1017/cbo9780511525247.
[13] R. Street (Ed.), Technology and Applications of Amorphous Silicon, in: Springer Series in Materials Science, Springer, 1999.
[14] S.Y. Myong, L.S. Jeon, S.W. Kwon, Superstrate type flexible thin-film Si solar cells using flexible glass substrates, Thin Solid Films 550 (2014) 705–709, http://dx.doi.org/10.1016/j.tsf.2013.11.039.
[15] K. Liu, W. Yao, D. Wang, D. Ba, H. Liu, X. Gu, D. Meng, G. Du, Y. Xie, Y. Ba, A study of intrinsic amorphous silicon thin film deposited on flexible polymer substrates by magnetron sputtering, J. Non-Cryst. Solids 449 (2016) 125–132, http://dx.doi.org/10.1016/j.jnoncrysol.2016.07.019.
[16] S. Fernández, J.J. Gandía, E. Saugar, M.B. Gómez-Mancebo, D. Canteli, C. Molpeceres, Sputtered non-hydrogenated amorphous silicon as alternative absorber for silicon photovoltaic technology, Materials 14 (21) (2021) 6550, http://dx.doi.org/10.3390/ma14216550.
[17] M. Demirkan, L. Trahey, T. Karabacak, Low-density silicon thin films for lithium-ion battery anodes, Thin Solid Films 600 (2016) 126–130, http://dx.doi.org/10.1016/j.tsf.2016.01.029.
[18] T. Karabacak, M.T. Demirkan, Density modulated thin film electrodes, methods of making same, and applications of same, United States Patent N° US 10, 133, 148 B2. Date of Patent: Jun. 25, 2019, 2019, URL https://patents.google.com/patent/US10333148B2/en.
[19] F. Urbach, The long-wavelength edge of photographic sensitivity and of the electronic absorption of solids, Phys. Rev. 92 (5) (1953) 1324, http://dx.doi.org/10.1103/physrev.92.1324.
[20] A.R. Zanatta, I. Chambouleyron, Absorption edge, band tails, and disorder of amorphous semiconductors, Phys. Rev. B 53 (7) (1996) 3833–3836, http://dx.doi.org/10.1103/physrevb.53.3833.
[21] J.A. Dobrowolski, F.C. Ho, A. Waldorf, Determination of optical constants of thin film coating materials based on inverse synthesis, Appl. Opt. 22 (20) (1983) 3191, http://dx.doi.org/10.1364/ao.22.003191.
[22] D. Poelman, P.F. Smet, Methods for the determination of the optical constants of thin films from single transmission measurements: a critical review, J. Phys. D: Appl. Phys. 36 (15) (2003) 1850.
[23] E. Márquez, E. Saugar, J. Díaz, C. García-Vázquez, S. Fernández-Ruano, E. Blanco, J. Ruiz-Pérez, D. Minkov, The influence of Ar pressure on the structure and optical properties of non-hydrogenated a-Si thin films grown by rf magnetron sputtering onto room-temperature glass substrates, J. Non-Cryst. Solids 517 (2019) 32–43, http://dx.doi.org/10.1016/j.jnoncrysol.2019.04.034.
[24] E. Márquez, E. Blanco, C. García-Vázquez, J. Díaz, E. Saugar, Spectroscopic ellipsometry study of non-hydrogenated fully amorphous silicon films deposited by room-temperature radio-frequency magnetron sputtering on glass: Influence of the argon pressure, J. Non-Cryst. Solids 547 (2020) 120305, http://dx.doi.org/10.1016/j.jnoncrysol.2020.120305.
[25] E. Márquez, J.J. Ruíz-Pérez, M. Ballester, A.P. Márquez, E. Blanco, D. Minkov, S.M.F. Ruano, E. Saugar, Optical characterization of H-Free a-Si layers grown by rf-magnetron sputtering by inverse synthesis using Matlab: Tauc–Lorentz–Urbach parameterization, Coatings 11 (11) (2021) 1324, http://dx.doi.org/10.3390/coatings11111324.
[26] Y. Liu, N. Jehanathan, H. Yang, J. Laeng, SEM observation of the “orange peel effect” of materials, Mater. Lett. 61 (6) (2007) 1433–1435, http://dx.doi.org/10.1016/j.matlet.2006.07.045.
[27] C. Smit, R.A.C.M.M. van Swaaij, H. Donker, A.M.H.N. Petit, W.M.M. Kessels, M.C.M. van de Sanden, Determining the material structure of microcrystalline silicon from Raman spectra, J. Appl. Phys. 94 (5) (2003) 3582–3588, http://dx.doi.org/10.1063/1.1596364.
[28] P. Roura, J. Farjas, P.R. i Cabarrocas, Quantification of the bond-angle dispersion by Raman spectroscopy and the strain energy of amorphous silicon, J. Appl. Phys. 104 (7) (2008) 073521, http://dx.doi.org/10.1063/1.2990767.
[29] D. Beeman, R. Tsu, M.F. Thorpe, Structural information from the Raman spectrum of amorphous silicon, Phys. Rev. B 32 (2) (1985) 874–878, http://dx.doi.org/10.1103/physrevb.32.874.
[30] F. Orapunt, L.-L. Tay, D.J. Lockwood, J.-M. Baribeau, M. Noël, J.C. Zwinkels, S.K. O'Leary, An amorphous-to-crystalline phase transition within thin silicon films grown by ultra-high-vacuum evaporation and its impact on the optical response, J. Appl. Phys. 119 (6) (2016) 065702, http://dx.doi.org/10.1063/1.4941021.
[31] S. O'Leary, B. Fogal, D. Lockwood, J.-M. Baribeau, M. Noël, J. Zwinkels, Optical dispersion relationships in amorphous silicon grown by molecular beam epitaxy, J. Non-Cryst. Solids 290 (1) (2001) 57–63, http://dx.doi.org/10.1016/s0022-3093(01)00728-1.
[32] B. Fogal, S. O'Leary, D. Lockwood, J.-M. Baribeau, M. Noël, J. Zwinkels, Disorder and the optical properties of amorphous silicon grown by molecular beam epitaxy, Solid State Commun. 120 (11) (2001) 429–434, http://dx.doi.org/10.1016/s0038-1098(01)00422-7.
[33] M. Morita, T. Ohmi, E. Hasegawa, M. Kawakami, M. Ohwada, Growth of native oxide on a silicon surface, J. Appl. Phys. 68 (3) (1990) 1272–1281, http://dx.doi.org/10.1063/1.347181.
[34] S.H. Wemple, M. DiDomenico, Behavior of the electronic dielectric constant in covalent and ionic materials, Phys. Rev. B 3 (4) (1971) 1338–1351, http://dx.doi.org/10.1103/physrevb.3.1338.

[35] S.H. Wemple, Refractive-index behavior of amorphous semiconductors and glasses, Phys. Rev. B 7 (8) (1973) 3767–3777, http://dx.doi.org/10.1103/physrevb.7.3767.
[36] D.R. Penn, Wave-number-dependent dielectric function of semiconductors, Phys. Rev. 128 (5) (1962) 2093–2097, http://dx.doi.org/10.1103/physrev.128.2093.
[37] G. Hall, XXVIII. The electronic structure of diamond, Lond. Edinb. Dublin Phil. Mag. J. Sci. 43 (338) (1952) 338–343, http://dx.doi.org/10.1080/14786440308520164.
[38] D. Weaire, M.F. Thorpe, Electronic properties of an amorphous solid. I. A simple tight-binding theory, Phys. Rev. B 4 (8) (1971) 2508–2520, http://dx.doi.org/10.1103/physrevb.4.2508.
[39] E. Belin, C. Senemaud, Densities of states of semiconductors by soft X-ray spectroscopy, Superlattices Microstruct. 8 (2) (1990) 141–143, http://dx.doi.org/10.1016/0749-6036(90)90078-l.
[40] D. Campi, C. Coriasso, Prediction of optical properties of amorphous tetrahedrally bonded materials, J. Appl. Phys. 64 (8) (1988) 4128–4134, http://dx.doi.org/10.1063/1.341323.
[41] J. Tauc, R. Grigorovici, A. Vancu, Optical properties and electronic structure of amorphous germanium, Phys. Status Solidi b 15 (2) (1966) 627–637, http://dx.doi.org/10.1002/pssb.19660150224.
[42] J. Tauc, Optical properties of amorphous semiconductors, in: J. Tauc (Ed.), Amorphous and Liquid Semiconductors, Springer US, Boston, MA, 1974, pp. 159–220, http://dx.doi.org/10.1007/978-1-4615-8705-7_4.
[43] D. Aspnes, Optical properties of thin films, Thin Solid Films 89 (3) (1982) 249–262, http://dx.doi.org/10.1016/0040-6090(82)90590-9.
[44] S. Adachi, Optical Constants of Crystalline and Amorphous Semiconductors, Springer US, 1999, http://dx.doi.org/10.1007/978-1-4615-5247-5.
[45] S. Adachi, H. Mori, Optical properties of fully amorphous silicon, Phys. Rev. B 62 (15) (2000) 10158–10164, http://dx.doi.org/10.1103/physrevb.62.10158.
[46] W.B. Jackson, S.M. Kelso, C.C. Tsai, J.W. Allen, S.-J. Oh, Energy dependence of the optical matrix element in hydrogenated amorphous and crystalline silicon, Phys. Rev. B 31 (8) (1985) 5187–5198, http://dx.doi.org/10.1103/physrevb.31.5187.